2024 IEEE PES Innovative Smart Grid Technologies Europe (ISGT EUROPE) | 979-8-3503-9042-1/24/$31.00 ©2024 IEEE | DOI: 10.1109/ISGTEUROPE62998.2024.10863189

Sustainable and cost-effective microgrid sizing methodology for mining operations considering reliability and energy not-served

Shah Mohammad Mominul Islam
The University of Adelaide
Adelaide, Australia
shah.islam,

Hossein Ranjbar
The University of Adelaide
Adelaide, Australia
hossein.ranjbar,

S. Ali Pourmousavi
The University of Adelaide
Adelaide, Australia
a.pourm,

Wen L. Soong
The University of Adelaide
Adelaide, Australia
wen.soong@adelaide.edu.au

***Abstract*—Mining industries consume a significant amounts of energy from fossil fuels, increasing carbon emissions. This paper presents a framework for the design of sustainable microgrid systems for mining through the integration of renewable energy sources to maximise environmental and economic outcomes. The study evaluates the applicability of solar PV, wind turbines, battery storage and diesel generators through a cost-benefit analysis in terms of energy cost, emissions, and reliability. Key findings indicate that wind turbines, when combined with diesel generators, drastically reduce cost and emissions. This work also examines microgrid configurations that have a lower diesel generator capacity but offer near-perfect reliability. Such configurations have proven to be feasible, as the energy shortfall is minimal and manageable by existing mining resources, thus reducing both costs and emissions.**

***Index Terms*—Microgrid, Mining, Techno-economic, Demand Response, Cost-benefit**

I. Introduction

The energy consumption in the mining industry is heavily reliant on fossil fuel sources in which only 0.001% of the total energy mix in 2014, was from renewable energy sources (RES) like solar and wind [1], [2]. The capacity of RES in nearly 80 mining enterprises increased from 1,066 MW in 2015 to 5,000 MW by 2019, driven by global decarbonisation and changes in energy subsidies, including increased RES subsidies and the goal of reducing fossil fuel subsidies by 50% by 2030 [4].

The mining sector, contributing 4-7% of global greenhouse gas (GHG) emissions, faces high and volatile diesel prices in remote operations [5]. Thus, the top 40 mining companies reduced GHG emissions by 3-5% using RES in mining microgrids (MGs) due to pressure from the government, investors and society during 2019-2020. Despite these benefits, a techno-economic framework is needed for optimal RES sizing for cost-benefit analysis within the energy mix [6].

While existing research offers cost-benefit analyses for typical MG sizing (e.g., [7]–[10]) for community and industrial use, a limited literature exists on MG applications in mining. However, a mining-specific MG design is highly required due to the unique operational and environmental factors of mining, as highlighted in Table I. Ref. [11] explored MG integration in mining to improve efficiency and reduce environmental impacts, but reliability issues in varying conditions are often overlooked. A hybrid MG sizing framework with RES and battery energy storage system (BESS) was developed based on HOMER Grid software in [12] and validated by three case studies in Australia. However, HOMER supports only monthly averages with hourly resolution, not detailed daily load data [13]. Ref. [14] studied DC/AC MG in mining, focusing on control strategies for stable load sharing to improve resilience and sustainability, but did not provide cost and emissions analysis, crucial for economic and environmental viability.

To the best of the authors' knowledge, a comprehensive techno-economic analysis using a detailed cost model that (1) incorporates the lifetimes of components in a MG for replacement cost and salvage value; (2) considers warranty periods for components of a MG; (3) accounts for environmental aspects of renewable MGs customised for mining; and (4) is supported with practical case studies has not been performed. This paper presents a framework for sizing and selecting MG components at remote mining sites, enabling a trade-off analysis between net present cost (NPC), emissions and reliability. This framework allows comparison with fossil fuel-dependent operations, previously unexplored in mining MG studies [11]–[13]. Besides, this work develops a comprehensive cost and emission models for MG components to provide a thorough techno-economic and environmental analyses in integrating RES and BESS. The framework is demonstrated using real-world mine in terms of load data, site-specific meteorological data, and current market cost indicators. Here are the key contributions of the paper:

- Develop detailed cost and emission models of MG components such as PV, wind, BESS, and diesel generators (DGs) including capital, operational, fuel, and replacement costs, as well as the emissions, salvage value, warranty period, and battery degradation.
- Develop an innovative framework for MG sizing trade-offs among NPC, emissions, and reliability is being introduced in which the energy generation data of each MG component are analysed, and small load curtailment is allowed to realise a lower cost MG design

The rest of the paper is organised as follows: Section II outlines the methodology, including the scenario-based MG

This project is supported by the Australian Government Research Training Program (RTP) through University of Adelaide Research Scholarship (UARS), with supplementary funding from the Mine Operational Vehicle Electrification (MOVE) project, funded by the Future Battery Industries Cooperative Research Centre (FBICRC) under the Commonwealth CRC Program, Australia.

979-8-3503-9042-1/24/$31.00 ©2024 Crown

Authorized licensed use limited to: University of Adelaide. Downloaded on April 28,2025 at 06:20:12 UTC from IEEE Xplore. Restrictions apply.

TABLE I
COMPARISON BETWEEN TYPICAL MICROGRIDS AND MINING MICROGRIDS

Criterion	Power Demand	Location	Grid Access	Main Focus
Typical MG	Low	Urban	Mostly	Cost optimisation
Mining MG	High	Remote	Rarely	Cost, reliability and emissions

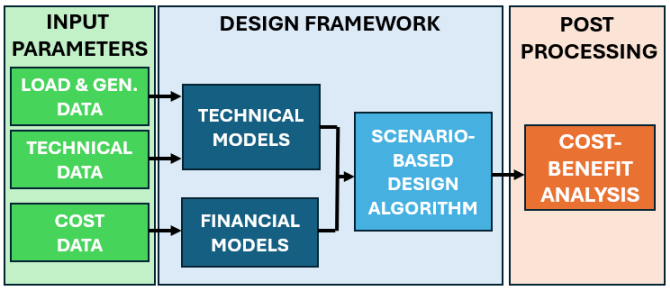

Fig. 1. Microgrid design framework.

design framework, the simulation algorithm, and the cost and emission models. Section III presents the results of the case study, discussing various combinations of MGs, their cost and emission trade-offs, and an analysis of MG reliability and unmet energy demand. Section IV concludes with a summary of the findings and future research implications.

II. METHODOLOGY

A. Scenario-Based MG Design

Figure 1 illustrates the proposed design framework for MG in mines in a three-layer approach: input parameters, design framework, and post-processing. The input parameters layer is made up of data from loads (power demand), generation (normalised power according to solar irradiation and wind speed, details in the supplementary file [16]), technical data (technical parameters of MG components and DG emission), and cost data (cost assumptions of all the MG components).

The second layer, the design framework, integrates technical and financial models with a scenario-based algorithm (1) to calculate NPC, emissions, and reliability for each MG sizing scenario. This algorithm priorities solar PV, wind turbines, and BESS, and uses the DG only when necessary to optimise clean energy use and reliability. The post-processing layer categories design solutions, identifies Pareto front solutions, and performs cost-benefit and reliability analysis.

In Algorithm 1, t is timestep with cardinal of T. $NPW[t]$ and $NPV[t]$ are the normalised wind and solar power in timestep t, derived from the wind speed and solar irradiation of the mine site. PWT, PPV, P_{bat}, and E_{bat} are the rated power capacities for the wind turbine, solar PV system, and BESS, respectively. $P_{load}[t]$, $P_S[t]$, $P_W[t]$, $P_{ch}[t]$, $P_{dis}[t]$, $P_{DG}[t]$, $P_{cur}[t]$, and $P_{sh}[t]$ are the load demand, solar power, wind power, BESS charging and discharging powers, DG power, power curtailment and unmet power at timestep t, respectively. $SOC[t]$, $SOC_{init}^{[t-1]}$, η_{ch}, and η_{dis} represent the state of charge, the initial SOC with the SOC in the previous time step, and the efficiencies of charge and discharge of BESS, respectively.

Algorithm 1 MG design algorithm for every specified scenario

(Initialisation and net power calculation)
for $t = 0, 1, 2, 3$ **to** T **do**
  $P_W[t] \leftarrow NPW[t] \times \text{PWT}$; $P_S[t] \leftarrow NPV[t] \times \text{PPV}$
  $P_{net}[t] \leftarrow P_{load}[t] - P_S[t] - P_W[t]$
  (Battery charge/discharge decision)
  if $P_{net}[t] > 0$ **then**
    $P_{ch}[t] \leftarrow 0$; $P_{dis}[t] \leftarrow \min(P_{bat}, P_{net}[t])$
  else if $P_{net}[t] < 0$ **then**
    $P_{dis}[t] \leftarrow 0$; $P_{ch}[t] \leftarrow -\max(-P_{bat}, P_{net}[t])$
  else
    $P_{ch}[t], P_{dis}[t] \leftarrow 0$
  end if
  (Battery state of charge update)
  $SOC[t] \leftarrow SOC_{init}^{[t-1]} + \Delta T(P_{ch}[t] \cdot \frac{\eta_{ch}}{E_{bat}} - \frac{P_{dis}[t]}{\eta_{dis} \times E_{bat}})$
  if $SOC[t] \geq SOC_{max}$ **then**
    $SOC[t] \leftarrow SOC_{max}$
    $P_{ch}[t] = (SOC_{max} - SOC_{init}^{[t-1]}) \times \frac{E_{bat}}{\Delta T \times \eta_{ch}}$
  else if $SOC[t] \leq SOC_{min}$ **then**
    $SOC[t] \leftarrow SOC_{min}$
    $P_{dis}[t] = (SOC_{init}^{[t-1]} - SOC_{min}) \times E_{bat} \cdot \frac{\eta_{dis}}{\Delta T}$
  end if
  (Net power recalculation)
  $P_{net}[t] \leftarrow P_{load}[t] - P_S[t] - P_W[t] - P_{dis}[t] + P_{ch}[t]$
  (Curtailment and diesel generator management)
  if $P_{net}[t] \geq 0$ **then**
    $P_{cur}[t] \leftarrow 0$
    if $P_{net}[t] > P_{DGmax}$ **then**
      $P_{DG}[t] \leftarrow P_{DGmax}$; $P_{sh}[t] \leftarrow P_{net}[t] - P_{DG}[t]$
    else
      $P_{DG}[t] \leftarrow P_{net}[t]$; $P_{sh}[t] \leftarrow 0$
    end if
  else
    $P_{DG}[t] \leftarrow 0$; $P_{sh}[t] \leftarrow 0$; $P_{cur}[t] \leftarrow -P_{net}[t]$
  end if
  (Final net power calculation)
  $P_{net}[t] \leftarrow P_{load}[t] - P_S[t] - P_W[t] - P_{dis}[t] + P_{ch}[t] - P_{DG}[t]$
end for

B. MG Components Cost and Emissions Models

This section presents the cost and emissions models for the MG components used in the design algorithm. These models calculate the total NPC for each MG technology based on capital, operational, and replacement costs, as well as salvage value. For simplicity, various combinations of MG components are used without scenario indices. Two types of BESS are considered: lithium-ion (Li) and redox-flow (Rf) batteries. The NPC, operational cost, and salvage value models for each MG component $\psi = \{PV, WT, Li, Rf, DG\}$ are calculated using the following equations:

$$C_N^{\psi} = C_C^{\psi} + C_O^{\psi} + C_R^{\psi} - C_S^{\psi} \tag{1}$$

Authorized licensed use limited to: University of Adelaide. Downloaded on April 28,2025 at 06:20:12 UTC from IEEE Xplore. Restrictions apply.

where C_C^{ψ}, C_O^{ψ}, and C_R^{ψ} represent the total capital, operational, and replacement costs of each MG component throughout the life, and C_S^{ψ} represents the total salvage value at the end of the MG's life. The general formula for calculating the operational cost (C_O^{ϕ}) and salvage value (C_S^{ψ}) of each MG component are as follows:

$$C_O^{\psi} = \sum_{y=1}^{L_{mg}} \frac{P_{\phi} \cdot c_{u,O}^{\phi}}{(1+i)^y} \tag{2}$$

$$C_S^{\psi} = C_{\xi} \cdot \left(1 - \frac{2}{L_{\xi}}\right)^{L_{\xi}^{used}} \cdot d \tag{3}$$

where P_{ϕ} is the power capacity of the MG component, $c_{u,O}^{\phi}$ is the per unit operational cost of MG component, L_{mg} is the total MG life and i is the interest factor. Also, C_{ξ} and L_{ξ} are the capital cost of the component and the expected life of the component while L_{ξ}^{used} is the duration it has been used in operation (typically the MG life) and d is the discount factor.

1) Solar PV systems

The NPC of the solar PV system (C_N^{PV}) is calculated using (1) where its capital cost can be expressed as:

$$C_C^{PV} = \sum_{k \in K} C_k; \forall k \in \{\mathtt{md}, \mathtt{in}, \mathtt{ld}, \mathtt{st}, \mathtt{cb}, \mathtt{ts}, \mathtt{tr}\} \tag{4}$$

where $\sum_{k \in K} C_k$ is the sum of the cost of modules (md), inverters (in), lands (ld), structures (st), cables (cb), tracking system (ts) and transformers (tr). The capital costs of modules and inverters, C_j, are calculated as:

$$C_j = c_j \cdot N_j; \forall j \in \{\mathtt{md}, \mathtt{in}\} \tag{5}$$

where c_j is the per unit cost of modules (md) and inverters (in), respectively. N_j is the number of modules and inverters that are calculated as:

$$N_{\mathtt{md}} = \left\lceil \frac{P_{DC}^{nom}}{P_{\mathtt{md}}} \right\rceil; N_{\mathtt{in}} = \left\lceil \frac{P_{AC}^{nom}}{S_{\mathtt{in}} \cdot pf} \right\rceil; P_{AC}^{nom} = \eta_{\mathtt{in}} \cdot \left(\frac{P_{DC}^{nom}}{R_{\frac{DC}{AC}}}\right) \tag{6}$$

where P_{DC}^{nom} and P_{AC}^{nom} are the nominal DC and AC power capacities of the installed solar PV system, respectively; $P_{\mathtt{md}}$ is the power capacity of each PV module; $\eta_{\mathtt{in}}$ is the efficiency of inverters, $R_{\frac{DC}{AC}}$ is the DC/AC ratio of solar PV system, $S_{\mathtt{in}}$ is the apparent power of the inverter, and pf is the inverter power factor. Total cost of land required to install PV modules ($C_{\mathtt{ld}}$), calculated as:

$$C_{\mathtt{ld}} = (c_{\mathtt{ld}}^u + c_{\mathtt{pt}}^u) \times (\alpha_{\mathtt{ld}} \cdot (N_{\mathtt{md}} \cdot l_{\mathtt{md}} \cdot w_{\mathtt{md}})) \tag{7}$$

where $c_{\mathtt{ld}}^u$ and $c_{\mathtt{pt}}^u$ are the cost of land lease and lightning protection, respectively. $l_{\mathtt{md}}$ and $w_{\mathtt{md}}$ are module dimensions, and $\alpha_{\mathtt{ld}}$ is area extension factor allowing additional space needed for inverters, transformers, cable channels, roads, ditches, and the control building. Other cost terms, i.e. the cost of the structure and tracking system, AC and DC cables, and transformers are calculated as follows:

$$C_k = c_k \cdot P_{DC}^{nom}; \forall k \in \{\mathtt{st}, \mathtt{ts}\} \tag{8}$$

$$C_C^c = \left(l_C^u \cdot \left(\frac{P_C^{nom}}{1000}\right)\right) \times c_C^u; \forall C \in \{\mathtt{DC}, \mathtt{AC}\} \tag{9}$$

$$C_{\mathtt{tr}} = c_{\mathtt{tr}} \cdot P_{AC}^{nom} \tag{10}$$

where c_k is the per unit cost of structures and tracking systems; c_C^u is the per unit cost of AC and DC cables, l_C^u is the per unit cable length cost and $c_{\mathtt{tr}}$ is the per unit cost of transformers.

The operational and replacement costs during the MG's life considering the life of the inverter ($L_{\mathtt{in}}$), and the warranty period of the PV modules ($Wr_{\mathtt{md}}$), which are unique to this study. The salvage value of each component in the PV system at the end of MG life, is calculated using (3).

$$C_O^{PV} = \sum_{y=1}^{L_{mg}} \frac{\alpha_O \cdot C_C^{PV}}{(1+i)^y} + \sum_{y=1}^{L_{mg}} \frac{\gamma_{is} \cdot C_C^{PV}}{(1+i)^y} \tag{11}$$

$$C_R^{PV} = \sum_{y=1}^{\lfloor \frac{L_{mg}}{L_{\mathtt{in}}} \rfloor} \frac{C_{\mathtt{in}}}{(1+i)^{y \cdot L_{\mathtt{in}}}} + \sum_{y=Wr_{\mathtt{md}}+1}^{L_{mg}} (f_{PV} \cdot N_{\mathtt{md}}) \cdot \frac{c_{\mathtt{md}}}{(1+i)^y} \tag{12}$$

$$C_S^{PV} = \sum_{k \epsilon K} C_k^S; \forall k \in \{\mathtt{md}, \mathtt{in}, \mathtt{ld}, \mathtt{st}, \mathtt{cb}, \mathtt{ts}, \mathtt{tr}\} \tag{13}$$

where α_O and γ_{is} are the operational and maintenance (O&M) and insurance cost factors, respectively, f_{PV} is the failure rate of PV modules.

2) Wind turbines

Similarly, the NPC of the wind system (C_N^{WT}) is calculated using (1). The capital cost of the wind system includes three terms as: cost of turbine (C_{tb}^{WT}), balance of system (C_{bs}^{WT}), and construction funding and contingencies (C_{cn}^{WT}), which are calculated as follows:

$$C_C^{WT} = C_{tb}^{WT} + C_{bs}^{WT} + C_{cn}^{WT} \tag{14}$$

$$C_{tb}^{WT} = \sum_{i \in I} c_i \cdot P_{WT}; \forall k \in \{\mathtt{rt}, \mathtt{nc}, \mathtt{tw}\} \tag{15}$$

$$C_{bs}^{WT} = \sum_{j \in J} c_j \cdot P_{WT}; \forall k \in \{\mathtt{eg}, \mathtt{pm}, \mathtt{fd}, \mathtt{sf}, \mathtt{it}, \mathtt{ei}\} \tag{16}$$

$$C_{cn}^{WT} = \sum_{k \in K} c_k \cdot P_{WT}; \forall k \in \{\mathtt{cf}, \mathtt{cy}\} \tag{17}$$

where P_{WT} is the power capacity of the wind system and c_i is the per unit costs of rotor (rt), nacelle (nc) and tower (tw); c_j is the per unit cost of engineering (eg), project management (pm), foundation (fd), site access facilities (sf), installation (it) and electrical infrastructure (ei); c_k is the per unit cost of construction funding (cf) and contingency (cy).

The operational cost and salvage value of the wind system are calculated using (2)and (3), while replacement costs are calculated considering only the rotor and nacelle replacements during the MG's lifespan as follows:

$$C_R^{WT} = \sum_{y=1}^{\lfloor \frac{L_{mg}}{L_{\mathtt{rt}}} \rfloor} \frac{C_{\mathtt{rt}}}{(1+i)^{y \cdot L_{\mathtt{rt}}}} + \sum_{y=1}^{\lfloor \frac{L_{mg}}{L_{\mathtt{nc}}} \rfloor} \frac{C_{\mathtt{nc}}}{(1+i)^{y \cdot L_{\mathtt{nc}}}} \tag{18}$$

where $L_{\mathtt{rt}}$ and $L_{\mathtt{nc}}$ are the lifetimes of the rotor and nacelle, respectively.

3) Battery Energy Storage Systems (BESS)

The NPC of the BESS (C_N^{BT}) is calculated using (1). The total capital cost includes two main terms related to energy capacity and power as:

$$C_C^{BT} = C_e^{BT} + C_p^{BT} \tag{19}$$

$$C_e^{BT} = \sum_{e \in E} c_e^u \cdot E_{BT}; \forall k \in \{\mathtt{ec}, \mathtt{bs}, \mathtt{si}, \mathtt{ep}, \mathtt{pd}\} \tag{20}$$

Authorized licensed use limited to: University of Adelaide. Downloaded on April 28,2025 at 06:20:12 UTC from IEEE Xplore. Restrictions apply.

$$C_p^{BT} = \sum_{p \in P} c_p^u \cdot P_{BT}; \forall k \in \{\mathtt{pc}, \mathtt{cc}\} \tag{21}$$

where E_{BT} and P_{BT} are the energy and power capacity of the BESS, and c_e^u represents the energy-related per unit cost, which includes energy capacity (ec), balance of system (bs), system integration (si), engineering and procurement (ep), and project development (pd). Similarly, c_p^u is the power-related per unit cost, which includes the power conversion system (pc) and control and communication (cc). The operational cost of the BESS during MG life is calculated using (2). The same equations in (19)–(21) apply to both Li and Rf batteries, though parameter values differ. The replacement cost of Li batteries depends on the degradation rate. In contrast, Rf batteries have higher operational costs due to annual electrolyte renewal or balancing, despite no degradation. The following equations (22), (23), (24), (25), (26), (27) present the replacement cost of Li batteries ($C_R^{BT,Li}$), which includes the replacement cost of power capacity (C_{Rp}^{BT}) and energy capacity ($C_{Re}^{BT,Li}$).

$$C_R^{BT,Li} = C_{Rp}^{BT} + C_{Re}^{BT,Li} \tag{22}$$

$$C_{Rp}^{BT} = \sum_{y=1}^{\lfloor \frac{L_{mg}}{L_{\mathtt{IN}}^{BT}} \rfloor} \frac{C_{\mathtt{pc}}^{BT}}{(1+i)^{y \cdot L_{\mathtt{IN}}^{BT}}} \tag{23}$$

$$C_{Re}^{BT,Li} = \sum_{y=1}^{\lfloor \frac{L_{mg}}{L^{BT,Li}} \rfloor} \frac{C_{\mathtt{ec}}^{BT}}{(1+i)^{y \cdot L^{BT,Li}}} \tag{24}$$

$$L^{BT,Li} = \min(L_{cal}^{BT,Li}, L_{cyc}^{BT,Li}) \tag{25}$$

$$L_{cyc}^{BT,Li} = \frac{1 - EoL}{e_{loss}^{yr}} \tag{26}$$

$$e_{loss}^{yr} = \beta_1 e^{\beta_2 (\frac{P_{BT}}{E_{BT}})} (n_{cyc}^{yr} \times DoD \times E_{cell}) \tag{27}$$

where $L^{BT,Li}$ is the life of Li batteries, determined by the minimum of calendar life ($L_{cal}^{BT,Li}$) and cycle life ($L_{cyc}^{BT,Li}$); EoL is the end-of-life fraction, and e_{loss}^{yr} is the annual energy loss percentage; β_1 and β_2 are the pre-exponential and exponential temperature function factors [15]; n_{cyc}^{yr} is the annual number of charge/discharge cycles; DoD is the depth of discharge; and E_{cell} is the energy capacity of each cell. The Rf battery replacement cost model, similar to Li batteries but excluding degradation, includes terms for energy and power components:

$$C_R^{BT,Rf} = C_{Rp}^{BT} + C_{Re}^{BT,Rf} \tag{28}$$

$$C_{Re}^{BT,Rf} = \sum_{y=1}^{\lfloor \frac{L_{mg}}{L^{BT,Rf}} \rfloor} \frac{C_E^{BT}}{(1+i)^{y \cdot L^{BT,Rf}}} \tag{29}$$

where C_{Rp}^{BT} is calculated by (23) and $L^{BT,Rf}$ is the life of the Rf batteries. The salvage value models of both the Rf and Li batteries are calculated as follows:

$$C_S^{BT} = C_{Se}^{BT} + C_{Sp}^{BT} \tag{30}$$

$$C_{Sp}^{BT} = [C_{pc}^{BT} \cdot \left(1 - \frac{2}{L_{\mathtt{IN}}^{BT}}\right)^{L_{us,\mathtt{IN}}^{BT}} + C_{bs}^{BT} \cdot \left(1 - \frac{2}{L_{bs}^{BT}}\right)^{L_{mg}}] \cdot d \tag{31}$$

$$C_{Se}^{BT} = C_e^{BT} \cdot \left(1 - \frac{2}{L^{BT}}\right)^{L_{us}^{BT}} \cdot d \tag{32}$$

where C_{Se}^{BT} and C_{Sp}^{BT} are the salvage values of the energy and power capacities, respectively. L^{BT}, $L_{\mathtt{IN}}^{BT}$, and L_{bs}^{BT} represent the battery cell, the inverter, and balance of system lifetimes, respectively. Also, L_{us}^{BT} and $L_{us,\mathtt{IN}}^{BT}$ are the number of years that the last battery pack and inverter have been used, respectively, that applies to both batteries as calculated below:

$$L_{us}^{BT} = L_{BT} - \left[\left(L_{BT} \times \lceil \frac{L_{mg}}{L_{BT}} \rceil\right) - L_{mg}\right] \tag{33}$$

$$L_{us,\mathtt{IN}}^{BT} = L_{\mathtt{IN}}^{BT} - \left[\left(L_{\mathtt{IN}}^{BT} \times \lceil \frac{L_{mg}}{L_{\mathtt{IN}}^{BT}} \rceil\right) - L_{mg}\right] \tag{34}$$

*4) **Diesel generators***

The NPC of the DGs is calculated using (1), where, operation cost (C_O^{DG}) and salvage value (C_S^{DG}) are determined using (2) and (3), respectively, while the capital (C_C^{DG}) and fuel costs (C_F^{DG}) are calculated as:

$$C_C^{DG} = P_{DG}^{max} \cdot c_{DG} \tag{35}$$

$$C_F^{DG} = \sum_{y=1}^{L_{mg}} \frac{l_{yr}^{DG} \cdot c_f^{DG}}{(1+i)^y} \tag{36}$$

$$l_{yr}^{DG} = \sum_{t=1}^{8760/\Delta T} (A \cdot P_{DG}^t + B) \Delta T \tag{37}$$

where P_{DG}^{max} is the maximum power capacity; c_{DG} is the per unit capital cost of the DG; c_f^{DG} is the fuel cost; and l_{yr}^{DG} is the annual diesel requirement. A and B are the parameters of the fuel consumption curve and ΔT is the time interval. Unlike other MG components, DGs produce operational emissions, calculated as follows:

$$EM_{DG} = \sum_{y=1}^{L_{mg}} l_{yr}^{DG} \cdot u_{L-GJ} \cdot em_{DG} \tag{38}$$

where em_{DG} is the per unit emission of the DG and u_{L-GJ} is the unit conversion factor.

This analysis evaluates trade-offs using net present Levelised Cost of Energy (LCOE) and per unit Emissions (EMpu), providing insight into the economic and environmental impacts of different combinations of MG components. This approach seeks an optimal balance between cost and sustainability. The LCOE and EMpu are calculated as follows:

$$LCOE = \frac{C_N^{PV} + C_N^{WT} + C_N^{BT} + C_N^{DG}}{E_{load} \times L_{mg}} \tag{39}$$

$$EMpu = \frac{EM_{DG}}{E_{load} \times L_{mg}} \tag{40}$$

where E_{load} is the total load demand served by all MG components.

III. Results and Discussion

The results in this section are from a case study of a typical mine site in Australia. Due to space limitations, the input parameters and the primary assumptions are discussed in the supplementary file [16].

A. Scenario-based MG Combinations

Different MG combinations with varying fractions of RES (PV and wind systems), BESS, and DG have been simulated to meet the energy demand of the mining site. Different technology combinations and sizes scenarios, includ-

Authorized licensed use limited to: University of Adelaide. Downloaded on April 28,2025 at 06:20:12 UTC from IEEE Xplore. Restrictions apply.

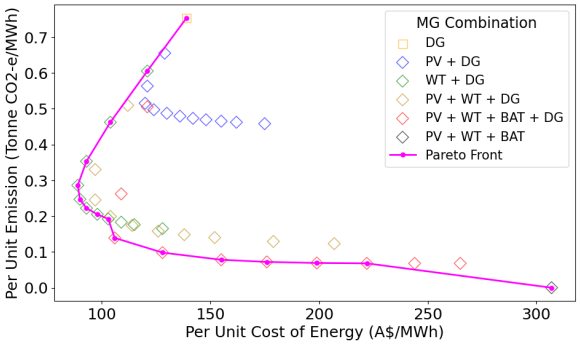

Fig. 2. Per unit cost vs emissions analysis for the scenario-based simulation study.

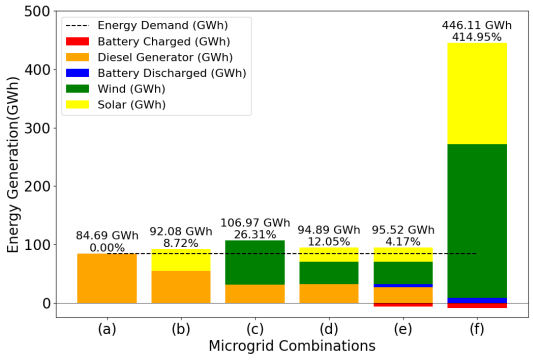

Fig. 3. Energy generation of microgrid combinations showing curtailment (%); (a) DG12, (b) DG12S15, (c) DG12W20, (d) DG12S10W10, (e) DG12S10W10B15/60, (f) S70W70B75/300.

ing the base case 'DG only'[DG12] have been considered, such as DG+PV [DG12S5..5..60] (means PV capacity starts at 5MW, each subsequent scenario has an increment of 5MW and maximum is 60MW), DG+WT [DG12W5..5..60], DG+PV+WT [DG12S5..5..60W5..5..60], DG+PV+WT+BAT [DG12S5..5..50W5..5..50B5/20..5/20..65/260], PV+WT+BAT [S70W70B75/300]. In this study, DG operates as a spinning reserve for scenarios without battery storage and with a 5MW/20MWh battery, as it cannot meet the 12MW peak load. For battery capacities greater than 12MW, DG is in cold start mode, reducing costs and emissions. The battery capacities are evenly divided between Li and Rf batteries, each with a 0.25-C rating. The required DG capacity is 12MW, which matches the peak demand as a backup.

B. Cost and Emissions Trade-off Analysis

Figure 2 compares emissions and costs for different MG scenarios. Data points represent various MG configurations. The pink Pareto front curve shows optimal trade-offs. As illustrated in Fig. 2, the combination of DG and WT provides the most optimal cases such that it can reduce both the LCOE and EMpu by 36% and 62%, respectively, proving renewable integration effectively optimises mining power systems.

C. Energy Generation of Microgrid Combinations

Figure 3 shows the energy generation mix and curtailment percentages for the least cost and emissions from each of the MG configurations of Fig. 2. Each bar represents combinations of a 12MW diesel generator (DG12), 10MW and 15MW PV (S10, S15), 10MW and 20MW wind (W10, W20),

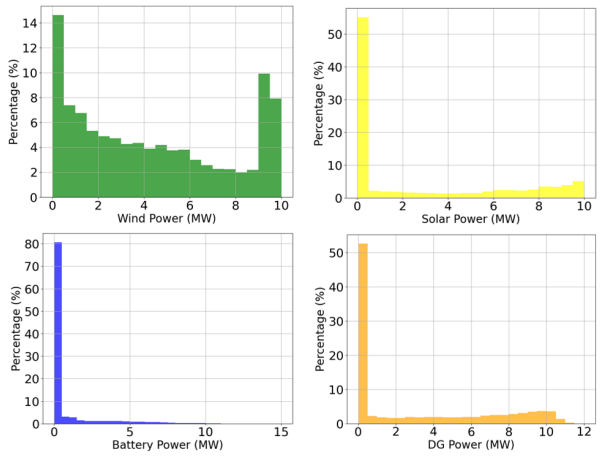

Fig. 4. Energy generation histogram analysis of DG12S10W10B15/60 scenario.

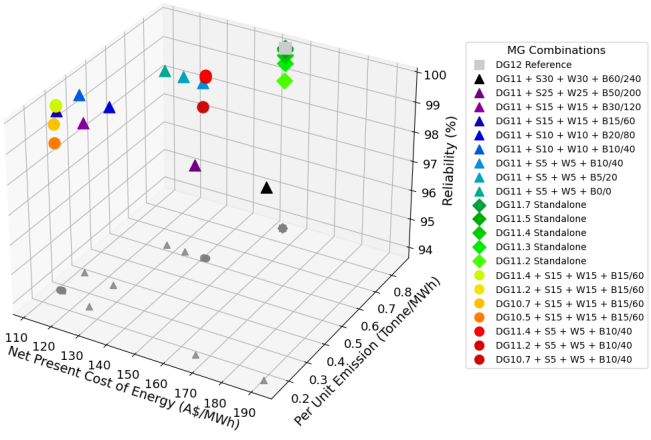

Fig. 5. Reliability, NPC and emissions analysis of the mining MG.

and 15MW/60MWh and 75MW/300MWh BESS (B15/60, B75/300). DG12 is the reference without renewables. The S70W70B75/300 combination shows high surplus and curtailment without DGs. Scenarios with higher renewables, such as S70W70B75/300, have substantial curtailment due to the variability of RES. Scenarios like DG12S15, with a backup DG, have a lower curtailment, which better matches demand. Properly sized batteries and renewables (DG12S10W10B15/60) significantly reduce curtailment.

Figure 4 shows the energy output histograms for the DG12S10W10B15/60 scenario from case (e) in Fig. 3. The analysis examines the economic impact of BESS and the environmental implications of the DG. Battery capacity, due to high storage costs, significantly affects system cost, while DG, as the sole emissions source, predominantly affects the environmental footprint. The goal is to optimise BESS and DG capacities by evaluating their utilisation rates. The results show that BESS is underused above 10MW, suggesting a 5MW reduction for cost savings. DG capacity drops significantly beyond 11MW, making a 1MW reduction viable to lower emissions. However, these changes may affect MG reliability and increase unmet energy demand. The next phase will

Authorized licensed use limited to: University of Adelaide. Downloaded on April 28,2025 at 06:20:12 UTC from IEEE Xplore. Restrictions apply.

TABLE II
REL(%), LCOE(A$/MWH), AND EM(TONNE/MWH) VALUES FOR VARIOUS MG COMBINATIONS

MG Combination	REL	LCOE	EM
DG11S15W15B30/120	99.89	125	0.23
DG11S15W15B15/60	99.82	113	0.26
DG11S10W10B20/80	99.78	125	0.35
DG11S10W10B10/40	99.78	113	0.37
DG11.4S15W15B15/60	100	113	0.26
DG11.2S15W15B15/60	99.96	113	0.26
DG12	100	139	0.753

investigate the impact on MG reliability and quantify 'energy not served (ENS)' to balance cost, emissions, and reliability.

D. MG Combinations Reliability Analysis

Figure 5 illustrates the interplay between reliability, NPC and emissions for scenarios in three contexts: (i) Varying BESS sizes with RES and fixed DG capacity, (ii) Variable DG capacities and (iii) Variable combinations of BESS, RES and DG capacities.

The objective is to assess how the reduction of DG or BESS capacities, along with RES, affects reliability. Figure 5 shows that the DG capacity is crucial for reliability, with minor reductions causing significant decreases compared to the BESS and RES adjustments. Several scenarios in Table II achieve substantially lower LCOE and emissions than the reference case (DG12 only) while maintaining near-perfect reliability.

Among configurations in Table II, DG11S15W15B15/60 is very practical with balanced sizes, reduced BESS, low cost and high reliability. Comparing DG11S15W15B15/60 and DG11S15W15B10/40 shows that the former has higher reliability and lower emissions at the same cost. The final part will analyse ENS for this MG configuration, assessing the frequency and duration of unmet energy events and quantifying them as a proportion of total load demand.

Figure 6 presents the ENS for the DG11S15W15B15/60 scenario. The *x-axis* categories instances by the number of consecutive 5-minute timesteps with unmet load demand. The left *y-axis* shows the frequency of these occurrences in a year, while the right *y-axis* represents the average percentage of unmet energy demand relative to the total load demand for these timesteps. This analysis shows that the MG configuration is highly reliable, with minimal unmet demand. This shortfall can be mitigated by slightly reducing ventilation system load or using alternative energy sources, such as batteries in electric trucks, to enhance the resilience and sustainability of the MG system.

IV. CONCLUSIONS AND FUTURE WORK

This research presented a framework for analysing RES integration into MGs in the mining industry, focusing on cost, emissions, and reliability trade-offs. Integrating solar PV, wind turbines, BESS, and DGs shows benefits, with a mixture of wind and DGs offering the lowest cost and emissions. The study highlights the balance between reducing DG capacity and maintaining reliability, noting that changes in DG capacity significantly affect the reliability of MG. Future studies will explore using mobile energy storage systems, such as electric haul trucks, to address unmet power demands, aiming for optimised battery coordination and improved system sustainability.

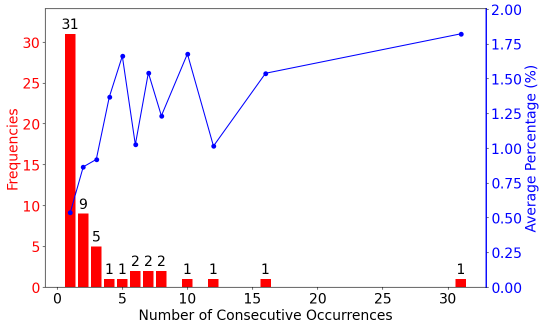

Fig. 6. Energy not served (ENS) occurrences and average percentage of ENS to load demand for DG11S15W15B15/60 combination with 99.82% reliability.

REFERENCES

[1] N. Maennling and P. Toledano, "The renewable power of the mine: Accelerating renewable energy integration," Columbia Cen. Sustain. Inv., New York, NY, USA, Tech. Rep., Dec. 2018.

[2] Y. Choi and J. Song, "Review of photovoltaic and wind power systems utilized in the mining industry," Ren. Sustain. Energy Rev., vol. 75, pp. 1386-1391, Aug. 2017.

[3] Rocky Mountain Institute, "Renewable Resources at Mines Tracker," 2019. [Online] Date of access: 20/02/2024. Available: https://rmi.org/our-work/industry-and-transportation/material-value-chains/renewable-resources-at-mines-tracker/

[4] M. Taylor, "Energy subsidies: Evolution in the global energy transformation to 2050," Int. Ren. Energy Agency, Abu Dhabi, UAE, Staff Tech. Paper, 2020.

[5] McKinsey, "Climate Risk and decarbonisation: What Every Mining CEO Needs to Know," 2020.

[6] PwC, "Mine 2019: Resourcing the Future," 2019. [Online] Date of access: 27/02/2024. Available: https://www.pwc.com.au/industry/mining/mine_2019.pdf

[7] S. S. Ullah, F. Ferdowsi, and T. Chambers, "Cost-Aware Strategies for Enhancing Energy Resilience in Microgrids via Stationary and Mobile Resources."Eng. Arch., 2024.

[8] A. Elmouatamid, M. A. Chowdhury, M. Netto, and P. W. Pong, "Economic feasibility study of standalone community microgrid in 37 cities of the USA," Trans. Hong Kong Inst. Eng., vol. 31, no. 1, pp. 20220027, 2024.

[9] R. Elazab, A. T. Abdelnaby, and A. A. Ali, "A comparative study of advanced evolutionary algorithms for optimizing microgrid performance under dynamic pricing conditions," Sci. Rep., vol. 14, no. 1, pp. 4548, 2024.

[10] A. Bhatraj, E. Salomons, and M. Housh, "An optimization model for simultaneous design and operation of renewable energy microgrids integrated with water supply systems," Appl. Energy, vol. 361, pp. 122879, 2024.

[11] J. S. Gómez, et al., "An overview of microgrids challenges in the mining industry," IEEE Access, vol. 8, pp. 191378-191393, 2020.

[12] O. Ellabban and A. Alassi, "Optimal hybrid microgrid sizing framework for the mining industry with three case studies from Australia," IET Ren. Power Gen., vol. 15, no. 2, pp. 409-423, 2021.

[13] O. Morales, "Homer® pro version 3.7 User Manual," Academia.edu, Dec. 2017.

[14] G. Mirzaeva and D. Miller, "DC and AC microgrids for mining applications," in Proc. IEEE IAS Petr. and Chem. Indus. Tech. Conf. (PCIC), 2022.

[15] J. Wang, J. Purewal, P. Liu, J. Hicks-Garner, S. Soukazian, E. Sherman, and M. W. Verbrugge, "Degradation of lithium ion batteries employing graphite negatives and nickel–cobalt–manganese oxide+ spinel manganese oxide positives: Part 1, aging mechanisms and life estimation," J. Power Sources, vol. 269, pp. 937-948, 2014.

[16] Supplementary document. [Online]. Available: http://dx.doi.org/10.13140/RG.2.2.11454.50240

Authorized licensed use limited to: University of Adelaide. Downloaded on April 28,2025 at 06:20:12 UTC from IEEE Xplore. Restrictions apply.